Available online at www.sciencedirect.com

ScienceDirect

Scripta Materialia 100 (2015) 98–101

Scripta MATERIALIA

www.elsevier.com/locate/scriptamat

Grain boundary formation by remnant dislocations from the de-twinning of thin nano-twins

Y. Cao,[a,b] Y.B. Wang,[a] X.H. An,[a] X.Z. Liao,[a,*] M. Kawasaki,[c,d] S.P. Ringer,[a,e] T.G. Langdon[c,f] and Y.T. Zhu[g,h]

[a]*School of Aerospace, Mechanical and Mechatronic Engineering, The University of Sydney, Sydney, NSW 2006, Australia*
[b]*School of Mechanical and Manufacturing Engineering, The University of New South Wales, Sydney, NSW 2052, Australia*
[c]*Departments of Aerospace & Mechanical Engineering and Materials Science, University of Southern California, Los Angeles, CA 90089-1453, USA*
[d]*Division of Materials Science and Engineering, Hanyang University, 17 Haengdang-dong, Seongdong-gu, Seoul 133-791, South Korea*
[e]*Australian Centre for Microscopy & Microanalysis, The University of Sydney, Sydney, NSW 2006, Australia*
[f]*Materials Research Group, Faculty of Engineering and the Environment, University of Southampton, Southampton SO17 1BJ, UK*
[g]*Department of Materials Science and Engineering, North Carolina State University, Raleigh, NC 27695, USA*
[h]*School of Materials Science and Engineering, Nanjing University of Science and Technology, Nanjing 210094, China*

Received 17 September 2014; revised 1 January 2015; accepted 2 January 2015
Available online 14 January 2015

We report a grain boundary formation mechanism in face-centred cubic metals with low stacking fault energies. Severe plastic deformation produces primary nano-twins with a twin boundary spacing of several nanometres, followed by secondary twinning through the activation of Shockley partial dislocations. The partial dislocations interact with primary twin boundaries, resulting in de-twinning of the primary twins and producing very high densities of sessile dislocations. The accumulation of these dislocations produces new grain boundaries with neighbouring grains having similar orientations.

Keywords: Grain boundary; Twinning; De-twinning; Grain refinement; Steel

In the last decades, extensive efforts have been devoted to understanding severe plastic deformation (SPD) induced grain refinement and deformation mechanisms [1–5]. It is well accepted that dislocation activities [6–9] and deformation twinning [10,11] are the two major grain refinement mechanisms. For face-centred cubic (fcc) metals with high SFE, SPD-induced grain refinement occurs via dislocation activities, including dislocation nucleation and multiplication, accumulation, interaction, tangling and spatial rearrangement [6,9,12]. Conversely, for fcc metals with relatively low SFE, stacking faults (SFs) and twin boundaries (TBs) play a key role in the grain refinement process [13–17]. Primary SFs and TBs block the motion of dislocations, leading to the accumulation of a high density of dislocations at the SFs and TBs that transforms the original atomically-flat coherent SFs and TBs into curved incoherent high-angle grain boundaries (GBs) [11,13,14]. As such, the finest grain size is largely determined by the smallest TB spacing or the smallest distance between neighbouring SFs/TBs [13,14].

Recent investigations on the HPT processing of a duplex stainless steel with fcc austenite having a very low SFE and body-centred cubic ferrite show that the average primary TB spacing in the austenite is ~7 nm [17]. Based on the grain refinement mechanism presented earlier for fcc phases with low SFE [13], where the interactions between dislocations and TBs transform coherent TBs into incoherent high-angle GBs, the smallest average grain size would be ~7 nm. However, the smallest average grain size was ~23 nm [17], thereby indicating that the mechanism is not applicable in the austenite. To understand the grain refinement mechanism operating in the austenite, detailed microstructural analyses were conducted on the austenitic phase in a duplex stainless steel processed by HPT to several strain levels. The present results reveal a hitherto unknown grain refinement mechanism that could apply to other fcc metals with low SFEs.

A commercial DP3W duplex stainless steel with a microstructure comprising ~50% volume fraction of both the fcc austenite and body-centred cubic ferrite was used in this research. The material was processed by quasi-constrained HPT [18] under 6 GPa applied pressure at room temperature for ¼, ½, and 1 revolution. The equivalent strain ε imposed by HPT was calculated using the relationship: $\varepsilon = \frac{2\pi Nr}{h\sqrt{3}}$, where N, r and h are the number of revolutions,

* Corresponding author. Tel.: +61 2 93512348; e-mail: xiaozhou.liao@sydney.edu.au

http://dx.doi.org/10.1016/j.scriptamat.2015.01.001
1359-6462/

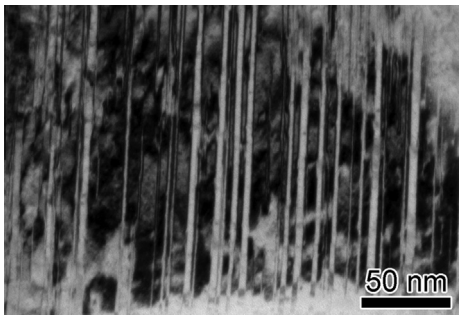

Figure 1. A typical TEM micrograph of the primary nano-twins formed in austenite grains at deformation stage 1.

the radial position, and the thickness of the disc sample, respectively [19]. Specimens for TEM investigation were carefully prepared using the standard mechanical grinding and electro-polishing methods described earlier [17]. A Philips CM12 TEM and a JEOL 3000F TEM were used for diffraction contrast imaging and high-resolution phase-contrast imaging, respectively.

The average grain size of the austenitic phase in the as-received material was ~8 μm. The austenite GBs were smooth and sharp and TBs were observed having spacings in the micrometre range. The estimated dislocation density in the as-received material was $\sim 5 \times 10^{13}$ m^{-2}. Depending on the microstructural features observed in this study, the deformation process was divided into three stages. At deformation stage 1, the HPT-imposed shear strain (ε) was smaller than ~3. In this stage, a high density of primary nano-twins with an average TB spacing of ~7 nm, based on TB spacings varying between ~1 and ~25 nm, and lengths of several micrometres was formed throughout all austenite grains, as shown in Figure 1. SFs and secondary nano-twins were rarely observed between primary TBs under detailed HRTEM analysis. The formation of a high density of primary nano-twins in coarse-grained austenite is attributed to the low SFE of the material (~26 mJ/m^2) and high external stress [20–24].

At the deformation stage 2, the shear strain value was between ~2 and ~5 and large numbers of secondary SFs and nano-twins inclined to the primary TBs were formed within the primary twin/matrix (T/M) lamellae, as shown in Figure 2. The long bands spanning across the whole image from the top-left to bottom-right in Figure 2(a) are primary T/M lamellae. Note that neither secondary SF nor secondary nano-twin were found within narrow lamellae with widths smaller than 7 nm: some of the narrow lamellae with no secondary nano-twin are marked with white arrows in Figure 2(a). A comparison between the primary TB-spacing (between ~1 and ~70 nm) at deformation stage 2 (Fig. 2(a)) and the primary TB-spacing (between ~1 and ~25 nm) at deformation stage 1 (Fig. 1) reveals an increase in the primary TB spacing. This gives evidence for the occurrence of de-twinning of the primary twins via interactions between partial dislocations and primary TBs, leading to a hierarchical nano-twined structure with a broadened primary TB-spacing. This phenomenon was also observed by Wei et al. [25] although there was no discussion of de-twinning.

Examples of the interactions are provided in Figures 2(b and c). For example, a high density of SFs (some of which are indicated by white arrows) were inclined to the primary TBs (marked with TB1) in Figure 2(b). The region enclosed by the two TB1 is a primary twin, the region enclosed by TB2 is a secondary twin, and the surrounding region is the matrix. A close examination of the primary twin indicates that the TB spacing on the left of TB2 is thinner than on the right by 7 {1 1 1} atomic layers, which is equivalent to the TB spacing of the secondary twin. At the intersection of the primary and secondary twins, the atomic arrangement is distorted by dislocations. The occurrence of dislocation/TB interactions at the intersection of the secondary and primary twins produced Shockley partial dislocations on 7 consecutive {1 1 1} atomic layers parallel to TB1 that slipped to the left (Fig. 2(b)), leading to de-twinning of the primary twin [26,27]. One dislocation at the top of TB1 in Figure 2(b) is marked by a black "T" and a magnified image of the local area surrounding the dislocation is shown in Figure 2(c). A close examination of the local distorted region magnified in Figure 2(c) reveals that a few consecutive atoms on a {1 1 1} plane are slightly distorted. The Burgers circuit in Figure 2(c) indicates the existence of the trailing partial dislocation of a SF (also marked by a black arrow in Figure 2(b)) immediately next to the dislocation. Therefore, various reactions may have occurred as the SF was driven towards the TB [28–30] and it is clear that some of these reactions can lead to the formation of new dislocations with Burgers vectors along other directions [29–31].

At deformation stage 3, the shear strain was between ~4 and ~11. Elongated grains with widths of less than ~200 nm and lengths of up to ~2 μm were formed in the austenite, as shown in Figure 3(a): one fully developed GB is marked with asterisks and two dislocation walls or low-angle GBs are indicated by two dashed lines. Detailed analysis of this microstructure reveals that the elongation direction of these grains is approximately parallel to the primary TBs, thus indicating a close relationship between the GBs and the primary T/M lamellae. Previous research suggested that coherent TBs can lose their coherency and transform into conventional GBs after trapping a large number of dislocations [13,15,16]. Based on this mechanism, two newly formed neighbouring grains should have an orientation relationship that is close to the twin relationship, i.e., a

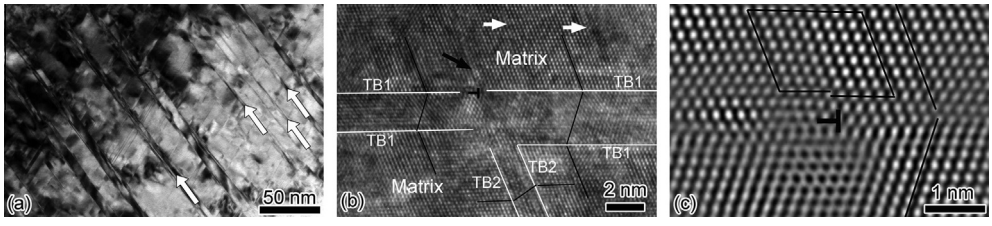

Figure 2. (a) A typical TEM micrograph showing the microstructures of secondary twinning within primary T/M lamellae; (b) a typical HRTEM image showing the de-twining to the primary twins via the interactions with secondary nano-twins/SFs; (c) a Fourier-filtered image showing the atomic arrangement around the dislocation marked by a black "T" in (b); a Burgers circle is drawn to help identify the partial dislocation.

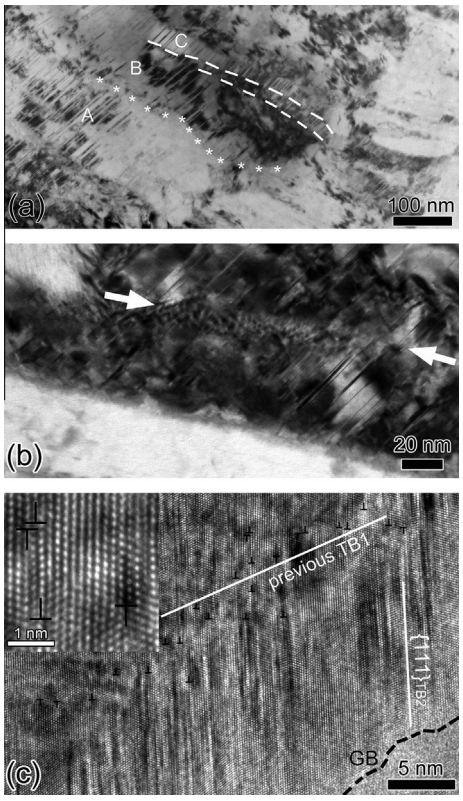

Figure 3. (a) A typical low magnification TEM micrograph showing the microstructures of elongated grains formed after the de-twinning of primary twins; (b) a high magnification TEM micrograph showing a dislocation wall within an elongated grain; (c) an HRTEM image showing a high density of dislocations aligned along the previous TB1 which is roughly parallel to the elongated grain boundary. The inset shows a magnified image of an area with dislocations.

misorientation angle of ~70.5° in fcc materials. However, neighbouring grains marked with A, B and C in Figure 3(a) all have similar orientations (their misorientation angles were less than 10°). Therefore, these GBs did not form via the previously reported mechanism [13,15,16]. A magnified image of a dislocation wall is shown in Figure 3(b) similar to those marked by dashed lines in Figure 3(a). The dislocation wall between the two white arrows is nearly parallel to the long GBs. It has been reported that dislocations can self-align to form GBs within a long and narrow twin lamella that subdivides the long twin band into smaller grains [14] and GBs formed in this way are usually perpendicular to the long TBs [14]. Therefore, we conclude that the dislocation walls in Figure 3 were not formed in this way.

Figure 3(c) shows a typical HRTEM image obtained from the dislocation wall area. A very high density of secondary nano-twins and SFs spans vertically in the image, and a large number of dislocations (marked by black "T") tend to align roughly parallel to the GB marked by the black dashed line at the bottom right of the image. None of the Burgers vectors of these dislocations is lying on the $\{1\,1\,1\}_{TB2}$ (marked by a straight white line) of the secondary nano-twins and SFs. A magnified image of a few dislocations is inserted at the top left corner of Figure 3(c). The intense secondary twinning activities on $\{1\,1\,1\}_{TB2}$ effectively block dislocation motion on the $\{1\,1\,1\}$ planes parallel to the previous TB1 (also marked by a straight white line). Therefore, the observed dislocations with Burgers vectors not lying on $\{1\,1\,1\}_{TB2}$ are formed through the interactions of partials on $\{1\,1\,1\}_{TB2}$ with previous TB1s [32,33]. Accordingly, it is reasonable to propose that, during the de-twinning process, extensive dislocation reactions with primary TBs occurred as shown in Figure 2 and as supported by the literature [16,28,30,34,35]. The dislocation reactions became more pronounced at the TBs of the thin primary twins while the matrix area was increased [16,36]. Eventually, the primary twins were depleted and numerous dislocations were left along the paths, thus forming dislocation walls as is clear from Figures 3(b and c). With further straining, these dislocation walls transform into conventional GBs after trapping more dislocations.

These results indicate the development of a new GB formation mechanism which is summarised in Figure 4 and operates by the complete de-twinning of nano-twins. The mechanism comprises three major stages. At stage 1, de-twining occurs in a grain containing a high density of primary nano-twins via secondary nano-twins/SF reactions with the primary TBs. As shown in Figure 4(a), when a leading partial of a secondary SF and/or a set of leading partials of a secondary nano-twin reach a primary TB, each leading partial dissociates into a stair-rod dislocation and a Shockley partial dislocation on the primary TB plane [30,34]. While the stair-rod dislocation/s remain in place, a single Shockley partial dislocation or a partial dislocation bundle (an incoherent TB) may move along the primary TB and this leads to de-twinning by one or a few atomic layers [30,34,37].

At stage 2, shown in Figure 4(b), further deformation produced more secondary nano-twins/SFs and more interactions with the primary twin at multiple places and this reduces significantly the thickness of the primary twins. As a result, the TBs gradually lose their ability to trap dislocations because, when the TB-spacing is critically small, the dislocation activities along the TBs dominate the plastic deformation instead of the dislocation slip transfer across TBs [16,36]. More dislocations with Burgers vectors parallel to the primary TB are created by the secondary nano-twins/SFs reacting with the primary TB (e.g., $\frac{1}{6}[2\bar{1}\,1]_M \rightarrow \frac{1}{6}[1\bar{2}\,1]_{TB} + \frac{1}{6}[1\,1\,0]_{TB}$, where subscripts "M" and "TB" represent matrix and TB, respectively) [30,34] or from the

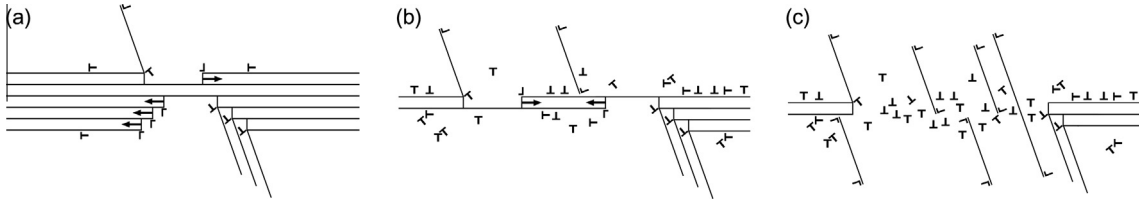

Figure 4. A schematic illustration of the GB formation mechanism by the depletion of a nano-twin: (a) dislocation-TB reactions causing de-twining to a primary twin; (b) a primary twin is nearly depleted; (c) a primary twin is completely depleted and a high density of dislocations is left along the path of de-twining to form a dislocation wall which blocks in-coming secondary nano-twins/SFs. The dislocation wall will later transform into a low angle GB.

dissociation of the previously trapped dislocations (e.g. $\frac{1}{2}[1\,0\,1]_{TB} \rightarrow \frac{1}{6}[0\,1\,1]_{T} + \frac{1}{6}[1\,1\,\bar{2}]_{TB}$, where subscript "T" represents twin) [16,34,38]. This is apparent from the microstructures shown in Figure 2 and the high dislocation density of $\sim 9.2 \times 10^{16}\ m^{-2}$ at the corresponding deformation stage.

At stage 3, shown in Figure 4(c), the primary nano-twin is fully de-twinned, and a large number of dislocations remain along the path. These dislocations, many of them sessile, act as barriers for further dislocation motion. Therefore, they trap more dislocations during further deformation, and gradually they transform the region into a low-angle GB. This is demonstrated by the high dislocation density apparent in Figure 3(c) and the measurement of the dislocation density as $\sim 1.7 \times 10^{17}\ m^{-2}$.

There is, however, a necessary condition for the occurrence of this GB formation mechanism by complete de-twinning of nano-twins. This condition is that the TB-spacing must be within a critical width range to allow a full extended-dislocation to develop [33]. This critical width range depends on the SFE of the material and the flow stress and it appears to be ~7–200 nm in the present case. Further investigations are needed to determine the critical widths as a function of SFE and stress. If the TB-spacing is below the critical width, as shown in Figure 1, dislocations slip along TBs rather than slip across twins or the matrix [32,33]. Without the dislocations slipping across the twins or the matrix, there is no obstacle for the Shockley partials along the TBs, and therefore there is no dislocation tangling or dislocation wall formation [33]. In the early stages of the de-twining, where the twin morphology changed (Fig. 1 cf. Fig. 2), many twins are fully de-twinned without leaving any traces of a dislocation wall. Therefore, sufficient space may be created in matrices for the cross-slip of dislocations. At the later stage of the de-twinning, some nano-twins are de-twinned while leaving a long trace of dislocation walls as described by the current model. Subsequently, the elongated grains that form may have widths of up to ~200 nm rather than a few tens of nano-metres, as shown in Figure 3.

In summary, our experimental results lead us to propose a new GB formation mechanism that operates via the de-twinning of nano-twins. The discovery of this GB formation mechanism is significant for two reasons. First, it clarifies the observation that the remnant dislocations from dislocation-twin boundary reactions during the process of de-twinning at nano-twins can generate dislocation walls that form GBs. Therefore, the discovery is an important step towards a complete understanding of the twinning-assisted grain refinement process. Second, the GB formed by de-twinning of a nano-twin is a low-angle GB. This textural aspect must be considered when the mechanical properties and thermal stability of the alloy are designed because it is anticipated that the behaviour of these GBs will be significantly different from high-angle GBs [4].

This project is supported by the Australian Research Council (Grant No. DP120100510 (Y.C., Y.B.W. and X.Z.L.)), the National Science Foundation of the United States (Grant No. DMR-1160966 (M.K. and T.G.L.) and Grant No. DMR-1104667 (Y.T.Z.)), the European Research Council under ERC Grant Agreement No. 267464-SPDMETALS (T.G.L.) and the China 1000 Plan Program (Y.T.Z.).

[1] R.Z. Valiev, R.K. Islamgaliev, I.V. Alexandrov, Prog. Mater. Sci. 45 (2000) 103–189.
[2] N. Hansen, Scr. Mater. 51 (2004) 801–806.
[3] P.V. Liddicoat, X.-Z. Liao, Y. Zhao, Y. Zhu, M.Y. Murashkin, E.J. Lavernia, R.Z. Valiev, S.P. Ringer, Nat. Commun. 1 (2010) 63.
[4] X.C. Liu, H.W. Zhang, K. Lu, Science 342 (2013) 337–340.
[5] T.G. Langdon, Acta Mater. 61 (2013) 7035–7059.
[6] D.A. Hughes, N. Hansen, Acta Mater. 45 (1997) 3871–3886.
[7] Y. Estrin, L.S. Tóth, A. Molinari, Y. Bréchet, Acta Mater. 46 (1998) 5509–5522.
[8] F. Roters, D. Raabe, G. Gottstein, Acta Mater. 48 (2000) 4181–4189.
[9] A. Mishra, B.K. Kad, F. Gregori, M.A. Meyers, Acta Mater. 55 (2007) 13–28.
[10] J.W. Christian, S. Mahajan, Prog. Mater. Sci. 39 (1995) 1–157.
[11] N.R. Tao, K. Lu, Scr. Mater. 60 (2009) 1039–1043.
[12] X.Z. Liao, J.Y. Huang, Y.T. Zhu, F. Zhou, E.J. Lavernia, Philos. Mag. 83 (2003) 3065–3075.
[13] Y.B. Wang, X.Z. Liao, Y.H. Zhao, E.J. Lavernia, S.P. Ringer, Z. Horita, T.G. Langdon, Y.T. Zhu, Mater. Sci. Eng. A 527 (2010) 4959–4966.
[14] K. Wang, N.R. Tao, G. Liu, J. Lu, K. Lu, Acta Mater. 54 (2006) 5281–5291.
[15] Y. Zhang, N.R. Tao, K. Lu, Acta Mater. 56 (2008) 2429–2440.
[16] L. Lu, X. Chen, X. Huang, K. Lu, Science 323 (2009) 607–610.
[17] Y. Cao, Y.B. Wang, X.H. An, X.Z. Liao, M. Kawasaki, S.P. Ringer, T.G. Langdon, Y.T. Zhu, Acta Mater. 63 (2014) 16–29.
[18] R.B. Figueiredo, P.R. Cetlin, T.G. Langdon, Mater. Sci. Eng. A 528 (2011) 8198–8204.
[19] R.Z. Valiev, Y.V. Ivanisenko, E.F. Rauch, B. Baudelet, Acta Mater. 44 (1996) 4705–4712.
[20] M.A. Meyers, O. Vöhringer, V.A. Lubarda, Acta Mater. 49 (2001) 4025–4039.
[21] I. Gutierrez-Urrutia, D. Raabe, Acta Mater. 59 (2011) 6449–6462.
[22] R.J. McCabe, I.J. Beyerlein, J.S. Carpenter, N.A. Mara, Nat. Commun. 5 (2014) 7.
[23] S. Mahajan, Scr. Mater. 68 (2013) 95–99.
[24] D.R. Steinmetz, T. Jäpel, B. Wietbrock, P. Eisenlohr, I. Gutierrez-Urrutia, A. Saeed-Akbari, T. Hickel, F. Roters, D. Raabe, Acta Mater. 61 (2013) 494–510.
[25] Y. Wei, Y. Li, L. Zhu, Y. Liu, X. Lei, G. Wang, Y. Wu, Z. Mi, J. Liu, H. Wang, H. Gao, Nat. Commun. 5 (2014) 3580.
[26] V. Yamakov, D. Wolf, S.R. Phillpot, H. Gleiter, Acta Mater. 50 (2002) 5005–5020.
[27] J. Wang, O. Anderoglu, J.P. Hirth, A. Misra, X. Zhang, Appl. Phys. Lett. 95 (2009) 021908.
[28] Y.B. Wang, M.L. Sui, Appl. Phys. Lett. 94 (2009) 021909.
[29] C.S. Hong, N.R. Tao, X. Huang, K. Lu, Acta Mater. 58 (2010) 3103–3116.
[30] Y.T. Zhu, X.L. Wu, X.Z. Liao, J. Narayan, L.J. Kecskes, S.N. Mathaudhu, Acta Mater. 59 (2011) 812–821.
[31] Y.T. Zhu, X.Z. Liao, X.L. Wu, Prog. Mater. Sci. 57 (2012) 1–62.
[32] Y. Wei, Phys. Rev. B 83 (2011) 132104.
[33] Z.X. Wu, Y.W. Zhang, D.J. Srolovitz, Acta Mater. 59 (2011) 6890–6900.
[34] Z.X. Wu, Y.W. Zhang, D.J. Srolovitz, Acta Mater. 57 (2009) 4508–4518.
[35] S. Ni, Y.B. Wang, X.Z. Liao, R.B. Figueiredo, H.Q. Li, S.P. Ringer, T.G. Langdon, Y.T. Zhu, Acta Mater. 60 (2012) 3181–3189.
[36] X.Y. Li, Y.J. Wei, L. Lu, K. Lu, H.J. Gao, Nature 464 (2010) 877–880.
[37] J. Wang, N. Li, O. Anderoglu, X. Zhang, A. Misra, J.Y. Huang, J.P. Hirth, Acta Mater. 58 (2010) 2262–2270.
[38] Y.B. Wang, B. Wu, M.L. Sui, Appl. Phys. Lett. 93 (2008) 041906.